Journal of Catalysis 268 (2009) 60–67

Contents lists available at ScienceDirect

Journal of Catalysis

journal homepage: www.elsevier.com/locate/jcat

Platinum nanoparticles on Al_2O_3: Correlation between the particle size and activity in total methane oxidation

Irene E. Beck *, Valerii I. Bukhtiyarov, Ilya Yu. Pakharukov, Vladimir I. Zaikovsky, Vladimir V. Kriventsov, Valentin N. Parmon

Boreskov Institute of Catalysis, Lavrentieva ave., 5, 630090 Novosibirsk, Russia

ARTICLE INFO

Article history:
Received 24 July 2009
Revised 4 September 2009
Accepted 4 September 2009
Available online 7 October 2009

Keywords:
Platinum
Methane
Catalytic oxidation
Size effect
Nanoparticles

ABSTRACT

Catalytic activity of the size-controlled platinum nanoparticles supported on the acid-pretreated γ-alumina has been tested in complete methane oxidation under lean conditions. The mean sizes of platinum particles varied from 1.3 to 10 nm with the narrow size distribution (TEM data). It has been found that the reaction under study is strongly size sensitive. The size dependence of the specific catalytic activity is narrow and bell-shaped, with the maximum TOF value observed for the catalysts containing partially oxidized platinum with the mean particle sizes of about 2 nm. The observed strong size sensitivity is shown to originate from the size dependence of the apparent activation energy of the methane oxidation and/or the platinum oxidation state in the catalytically active nanoparticles.

1. Introduction

Catalytic combustion of methane has many applications, for example, as an alternative to the conventional thermal combustion or for the abatement of methane emissions from methane or natural gas combustion devices including lean-burn natural gas vehicles. At the same time, methane as the least reactive hydrocarbon is the most stable against oxidation. It has been, for example, found that the traditional three-way catalysts used for controlling the emissions from gasoline-powered vehicles are not able to remove methane completely at the working conditions both from automobile and from stationary combustion engine exhausts. Therefore, the search of catalysts active in total oxidation of methane at the relatively mild conditions is still the very actual task.

In this work we try to prepare such a catalyst on the basis of Pt particles supported on γ-Al_2O_3, with the mean size of the platinum particles being used as the main parameter for optimization of the catalyst performance. Platinum is known to be one of the most active metals for hydrocarbon oxidation and is comparable well with palladium in activity and stability. As a consequence, platinum supported on alumina is widely used for the oxidative removal of small amounts of hydrocarbons from gaseous or liquid streams.

On the other hand, catalytic activity of the supported Pt nanoparticles has been shown for a number of catalytic reactions to depend on the mean platinum particle size [1–3], the methane oxidation being the subject of many investigations. In spite of significant interest in the system, available literature data on this subject are rather contradictory [4–6]. E.g., for the methane oxidation at temperature range from 260 to 335 °C on four Pt/SiO_2 catalysts, approximately 30-fold increase in TOF with the reduction of platinum dispersion from 81% to 7% was reported [7]. For Pt/Al_2O_3 catalysts, this size effect has been reported either to be insignificant [8,9] or to cause a 4-fold (for the CH_4 oxidation at $T = 280$ [10] and 440 °C [5] at the Pt crystallite sizes, d, changed from 1 to 5 nm), 10-fold ($T = 450$ °C, d changed from 1 to 10 nm) [11], and even 200-fold ($T = 500$ °C, d varied from 1 to 35 nm) [12] increase in TOF with diminishing Pt particle sizes. It has been concluded that this increase in TOF is caused by significant changes either in activation energy [9], or in pre-exponential factor [5,12] or in both the factors [10] when the Pt particle size is varied.

It should be however noted that the great majority of catalysts studied in the cited papers have been prepared from the chloride-containing precursors and, thus, the catalysts were very likely contaminated with a significant amount of residual chlorine (for example, up to 0.8% in Ref. [11]), which is the well-known poison for oxidation catalysts [13]. The procedure of the catalyst heating, which was used for the preparation of the samples with larger Pt particles, can cause not only sintering of the Pt particles, but also a partial loss of chlorine impurities. Definitely, this would improve the catalyst performance. The last suggestion seems to be confirmed by the data of Burch and Loader who reported the independence of the specific rate on the particle size ranged from 1.4 to 3.7 nm at temperatures 425 to 500 °C for the Pt/Al_2O_3 catalysts

* Corresponding author. Fax: +7 383 330 83 56.
E-mail address: beck@catalysis.ru (I.E. Beck).

0021-9517/$ - see front matter © 2009 Elsevier Inc. All rights reserved.
doi:10.1016/j.jcat.2009.09.001

prepared from a chlorine-free precursor [6]. At the same time, they reported that the increase in the reaction temperatures to 525 to 550 °C has changed the tendency to a small increase in the reaction rate with raising particle size. A similar result is reported in [9], although the transition from independence of the catalytic activity on the Pt particle size at low temperatures to the size dependence at higher temperature is observed at lower temperature (430 °C).

Contrary to the papers cited above, a parabola-like pattern of the TOF–Pt particle size correlation with the maximal TOF for the catalysts with ca. 30% dispersity has been reported in [14–16]. This inconsistency in the literature data can originate from the non-uniformity in the size distribution of Pt particles on the carrier.

In this work, a convenient and reproducible method for the preparation of monodisperse chlorine-free Pt/γ-Al_2O_3 catalysts ensuring the narrow unimodal size distribution of platinum nanoparticles (HR TEM data) on the acid-pretreated γ-alumina surface has been elaborated. Using this method, a set of the samples differing in the mean sizes of the Pt particles has been prepared. This allowed the observation of a direct correlation between catalytic activity in the methane combustion and the platinum particle size.

2. Materials and methods

2.1. Catalysts preparation

A series of monodisperse alumina-supported Pt catalysts was prepared by the incipient wetness impregnation of the acetic acid-pretreated γ-Al_2O_3 as a support. The original γ-Al_2O_3 (Sasol TKA-432) was crushed and sieved to the grain sizes between 0.25 and 0.50 mm and then dried at 500 °C for 2 h (the BET surface area of 215 $m^2\ g^{-1}$). This fraction was treated by acetic acid using the incipient wetness method followed by overnight drying in air and for 8 h in an oven at 120 °C. The supports pretreated in this manner were then impregnated with aqueous platinum nitrate solutions, which were different on Pt-to-NO_3^- ratios, by the incipient wetness method. The resulting slurry was shaken before overnight drying in air and then in an oven at 120 °C for 4 h. Calcination of the impregnated support at 400 °C for 4 h or at 600 °C for 2 h followed by cooling in a desiccator finalizes the preparation procedure. According to AES with the inductively coupled plasma (Baird) the amount of platinum supported on γ-Al_2O_3 was similar (ca. 0.7 wt.%) for all the samples. The surface elemental composition (Al, O, and Pt, in the absence of unexpected impurities such as N and Cl) determined with X-ray photoelectron spectroscopy (VG ESCALAB HP spectrometer) and energy dispersing X-ray micro-analysis (JEM-2010) was also the same for all the samples.

2.2. Characterization of catalysts

Transmission electron microscopy (JEM-2010, Jeol Co.) was used to characterize the Pt particle size distribution on the support surface and to define the mean particle sizes for each synthesized sample. Prior the TEM examination, the samples were ground and suspended in ethanol. A drop of the suspension was then mounted on a copper grid covered by a "holed" carbon film, and the solvent was evaporated. All TEM measurements were performed at 200 kV and line-in-line resolution of 0.14 nm. Periodic images of the lattice structures on electron micrographs were analyzed using the digital Fourier transformation. The size distribution of the platinum crystallites was determined by measuring 200 to 700 particles for each sample. The mean Pt particle size values for the fresh catalysts established by TEM were used to reveal the size sensitivity in the methane oxidation. The absence of significant changes in the mean particle sizes in the course of the CH_4 oxidation reaction was random checked for several catalyst samples by TEM. Moreover, both specific surface areas and the pore volume distributions were similar for the fresh and the treated samples.

The EXAFS and XANES spectra of the Pt–L_3 edges for all the samples studied were measured at the Siberian Synchrotron Radiation Center (SSRC, Novosibirsk, Russia). The storage ring VEPP-3 with the electron beam energy of 2 GeV and the average stored current of ca. 100 mA has been used as the source of radiation. The X-ray energy was monitored with a channel cut Si(1 1 1) monochromator. XANES and EXAFS spectra were recorded with the steps of about 0.3 and 1.5 eV, respectively. All the spectra were recorded under transmission mode using two ionization chambers as detectors. The harmonics rejection was performed by using a SiO_2 mirror.

The EXAFS spectra were treated using the standard procedure [17] with "Viper" code [18]. The background was removed by extrapolating the pre-edge region onto the EXAFS region in the form of Victoreen's polynomials. Three cubic splines were used to construct the smooth part of the absorption coefficient. The inflection point of the edge of the X-ray absorption spectrum was used as initial point ($k = 0$) of the EXAFS spectrum. The radial distribution function (RDF) was calculated from the EXAFS spectra in $k^3\chi$ (k) as modulus of Fourier transform at the wave number intervals 3.0 to 12.5 $Å^{-1}$. The curve fitting procedure with EXCURV92 code [19] was employed to determine precisely the distances and coordination numbers in the similar wave number intervals after preliminary Fourier filtering with the use of known XRD data for the bulk compounds. The values of the Debye–Waller factors were fixed ($2\sigma^2 = 0.012\ Å^2$).

2.3. Catalysts testing

Catalytic activity of the Pt/γ-Al_2O_3 samples, which were different in the mean particle size, was measured as the specific stationary rate of the reaction using a conventional home-made gradientless flow-circulation reactor under oxidizing conditions, at a constant reactor temperature [20]. The catalyst (ca. 1 g) was placed in the steel flow-circulation reactor with internal diameter of 25 mm. The external flow-circulation pump provided the constant space velocity of the premixed reactants through the catalyst layer with more than 15 recirculations per minute thus providing the total mixing mode. Note, the analyzed outlet mixture in such the reactor is the same as the mixture over the operating catalyst. Before the rate measuring, a delay for more than 1.5 h at the chosen temperature and gas mixture composition was applied until the steady state rate is reached. The products were analyzed by gas chromatography. To separate methane and CO_2 in the outlet gas mixture, a carbon column was used. Carbon monoxide was never detected among the products.

The experiment was arranged as a set of "standard kinetic experiments" (SKE) for each catalyst. In such SKE the space velocity of the initial gas mixture (IGM) was varied from 50 to 1100 ml/min with the composition of IGM kept constant (1 vol.% CH_4, 20.8 vol.% O_2, N_2 as balance gas). The stationary rate of the reaction W ($ml_{CH_4}\ g_{cat}^{-1}\ s^{-1}$) was calculated for every given space velocity of IGM taking into account the composition of the outlet gas mixture (OGM) being at the same time the contacting reaction mixture under the steady-state conditions. The specific stationary reaction rate ($W_{0.5}$) at the same temperature and the composition of OGM (0.5 vol.% methane, 0.5 vol.% CO_2, 1 vol.% H_2O, 19.8 vol.% O_2) served as a criterion for the comparison of catalytic activities of different samples while a set of $W_{0.5}$ values measured at different temperatures for one sample was used for the estimation of apparent activation energy of methane oxidation. The gradientless flow-recirculation method used allows one to measure the stationary reaction rate without resorting to the assumption of reaction mechanism, first order in hydrocarbon, etc.

The stationary reaction rate was recalculated to the specific catalyst activity. The number of the surface Pt atoms was calculated in assumption that the metal particles are spherical and the dispersion value D_M (D, %/100) can be calculated from the surface mean particle size d_{Vs} ($\sum V_i/\sum S_i$, nm) using Eq. (1) [21]

$$D_M = 6 \cdot V_m / a_m \cdot d_{Vs}, \quad (1)$$

where V_m = atomic volume (nm^3) and a_m = average surface area occupied by one metal atom (nm^2).

In turn $V_m = M \cdot 10^{21}/\rho \cdot N_A = 0.0151$ nm^3 and $a_m = 1 \cdot 10^{14}/\sigma = 0.08$ nm^2, where M = molecular mass (195.09 g mol^{-1} for Pt), ρ = density of Pt (21.45 g cm^{-3}), N_A = the Avogadro's number (6.02×10^{23} atoms mol^{-1}), and σ = the concentration of the metal atoms on the surface (1.25×10^{15} atoms cm^{-2} for Pt).

3. Results and discussion

3.1. Size distribution of supported Pt nanoparticles

Details of the preparation procedure for all catalysts applied in this study are summarized in Table 1.

Two main parameters, which were varied during the preparation, were the molar ratio of the Pt precursor and nitrous acid in the impregnating solutions (the second column) and the calcination temperature of the impregnated samples (the third column).

The morphology of the prepared catalysts was characterized by TEM. Typical TEM micrographs of some samples are shown in Fig. 1, while the corresponding size distributions of platinum particles measured for the same four samples are shown in Fig. 2. One can see that the platinum particles visualized as dark spots (Fig. 1) are homogeneously dispersed on the alumina surface, the standard deviation from the mean particle diameter being about 25% for most samples (Fig. 2).

Another important conclusion, which follows from the data of Figs. 1 and 2, is that both the ratio of platinum to acid in the precursor solution and the calcination temperature (400 or 600 °C) have a great influence on the mean sizes of the platinum particles.

The mean sizes of Pt particles, as well as the values of dispersion (D_M) calculated according to Eq. (1) are also summarized in Table 1. Two main trends can be extracted from the TEM data (Figs. 1 and 2, Table 1). First of all, the increase in the concentration of nitric acid in the impregnating solution raises the mean size of the Pt particles and reduces the dispersion from 70% to 40%. The experiment with alkalization of the impregnating solution (sample IVa, Table 1) indicates that concentration of the nitrate anions rather than pH (compare samples IIIa and IVa, Table 1) is the crucial parameter for this trend. Furthermore, the increase in the calcination temperature enlarges platinum particles, this enlargement being more significant for the samples with smaller particles (compare samples Ia and Ib, IIa and IIb, and IIIa and IIIb).

Deviations from the above-mentioned trends (for instance, low-temperature calcined sample Va with the largest platinum particles was prepared from the precursor solution with the lowest concentration of nitric acid) are not understandable now and will be a subject of future investigations. In spite of these deviations, one can conclude that the used procedure of the catalyst preparation allows the control of the mean size of the γ-Al_2O_3-supported platinum particles in the range of 1 to 10 nm (Table 1).

Table 1
Some characteristics of the Pt/γ-Al_2O_3 catalysts under study.

Catalyst #	Precursor (Pt:HNO_3 ratio)	Calcination temperature (°C)	Metal loading (%)	d_{Pt} (nm)	D[a] (%)
Ia	1:1.5	400	0.69	1.3 ± 0.4 1.4 ± 0.4[b]	70.6
IIa	1:3.5	400	0.77	1.7 ± 0.4	60.4
IIIa	1:4.5	400	0.71	2.1 ± 0.4 2.1 ± 0.5[b]	52.3
IVa	1:4.5[c]	400	0.73	2.2 ± 0. 5	42.2
Va	1:0.5	400	0.75	2.5 ± 0.6	41.5
IIIb	1:4.5	600	0.71	2.8 ± 0.7	35.3
Vb	1:0.5	600	0.75	3.6 ± 0.6	29.6
IIb	1:3.5	600	0.77	6.4 ± 1.9	16.1
IVb	1:4.5[c]	600	0.73	8.5 ± 1.8 8.8 ± 1.7[b]	12.2
Ib	1:1.5	600	0.69	10.0 ± 2.6	9.7

[a] The dispersion value was calculated from TEM data on surface average particle sizes assuming the metal particles to be spherical.
[b] Data for catalysts aged under reaction conditions for 6 h.
[c] The precursor solution was alkalinized with tetramethylammonium hydroxide up to pH 8.5 and applied to unpretreated alumina.

3.2. Correlation between the size of Pt particles and methane oxidation activity

Catalytic properties of these catalysts are compared in Fig. 3 which presents the log W versus log C_{CH_4} dependences for a number of samples. One can see that these dependences can be linearized by straight lines for all the Pt/Al_2O_3 catalysts studied with the correlation coefficient of ca. 0.99 calculated of the least-square fit. The catalytic activity was then determined as the reaction rate, $W_{0.5}$ (see the horizontal dashed lines), at the 50% methane conversion. The inaccuracy in the values of catalytic activity determined by this manner increases for the samples with the biggest Pt particles (see Fig. 3, sample Vb), since 50% conversion is far from the range of measurable values and is determined via extrapolation of the describing line to the desired $W_{0.5}$ region.

Fig. 4 shows the dependence of the apparent turnover frequencies (TOFs) on the mean sizes of the Pt particles. The data obtained reveal a strong sensitivity of this parameter on the mean platinum particle sizes ranging between 1.3 and 10 nm. The maximal TOF value is observed for the catalyst with the mean Pt particle sizes of about 2 nm (Fig. 4). The catalysts with the Pt particles sized below and above 2 nm exhibit a trend of steeply decreasing the specific catalytic activity, respectively, with the reduction or increase of the mean particle size. A similar maximum in TOF was also observed in [14–16] at the Pt dispersion of 31% to 33%, although no direct TEM data on the mean sizes of platinum particles were available in those papers.

The reasons of the observed non-monotonous size effect are not completely understandable now and require an additional investigation of the state of the active component in the synthesized samples by physical methods. Indeed, the steep gradient of the TOF values from its maximum with the particle size diminishing is difficult to ascribe to geometric [22,23] or thermodynamic [24] factors only. Most probably, this behavior can be explained by the superposition of both electronic (a gradual change of features from non-metallic to metallic one with the particle size increase) and geometric (the ratio of edges, corners, steps, and other defects) factors. Namely, appropriate combination of metallic and oxidic platinum features has been suggested in [25,26] to be a key factor for high activity of platinum catalysts in methane oxidation. According to the molecular theory of structure sensitivity [1] the same type of surface sensitivity should be also expected if dissociative cleavage of C–H σ-bond is the rate-limiting step.

3.3. The size of Pt particles and activation energy

To make the first step in the study of the origin of the observed size effect, we have measured the apparent activation energy E_a of the methane oxidation for some sizes of the platinum particles. The E_a values were calculated from the slope of the linear approxima-

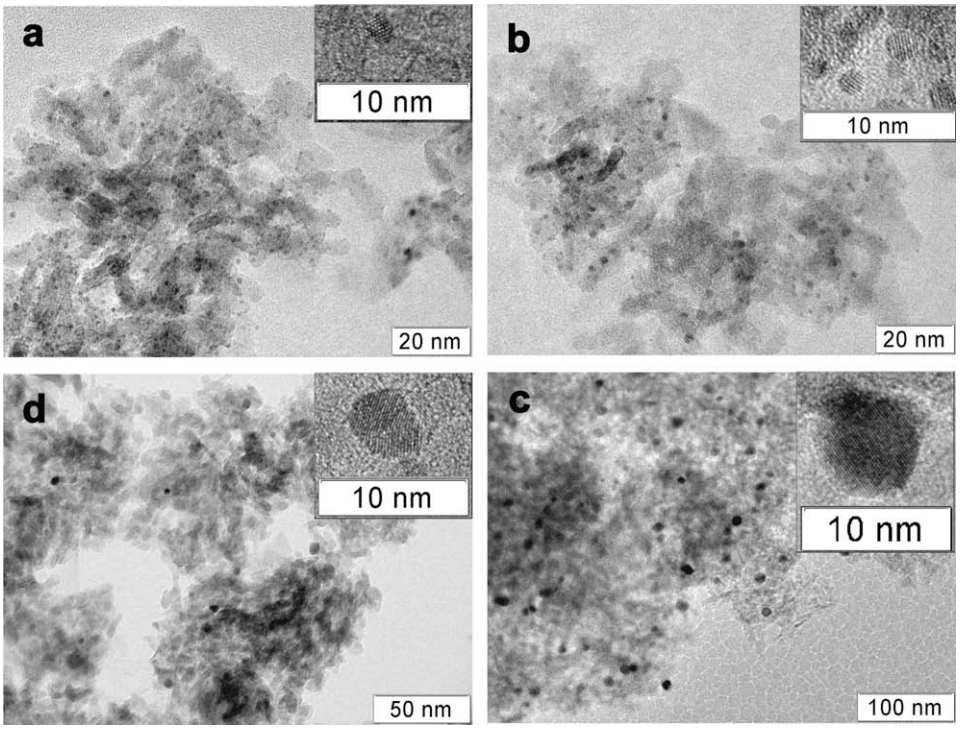

Fig. 1. Transmission electron micrographs for some 0.75%Pt/γ-Al_2O_3 catalysts of widely varying dispersity. The mean Pt particle size of 1.3 nm (a, sample Ia) and 2.0 nm (b, sample IIIa) was calculated for catalysts calcined at 400 °C, whereas 3.6 nm (c, sample Vb) and 8.5 nm (d, sample IVb) for catalysts calcined at 600 °C. The interplanar spacing ~2.27 Å on the inserted high resolution images correspond to the crystal lattice of metallic platinum displaying the (1 1 1) lattice planes.

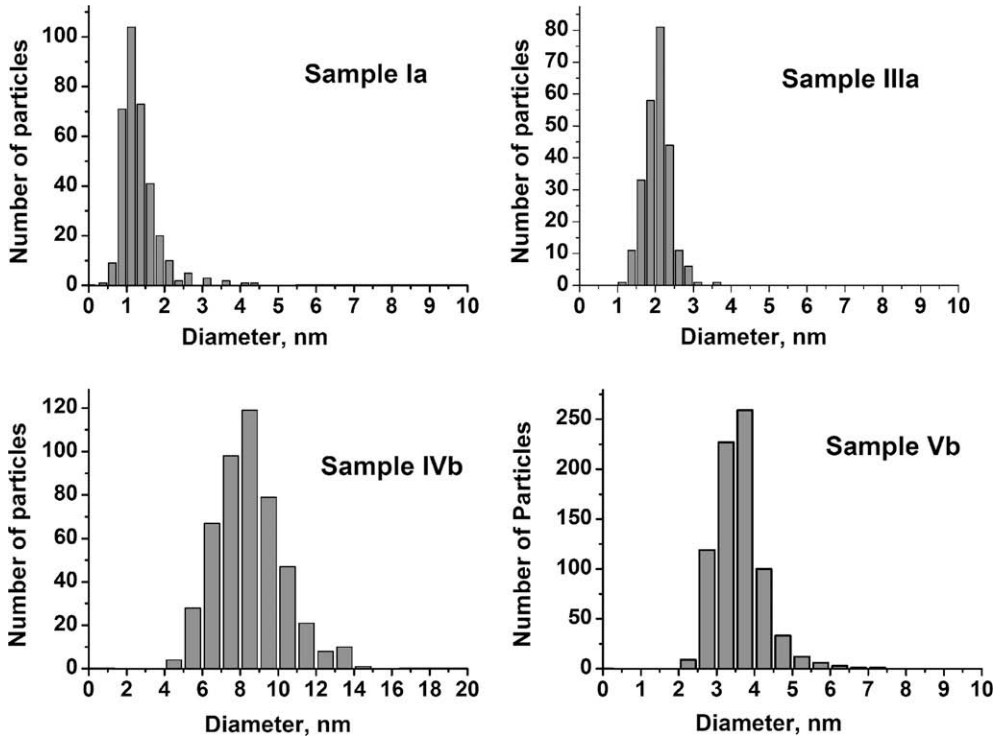

Fig. 2. Size distribution of Pt particles deposited on γ-Al_2O_3 for the same four 0.75%Pt/γ-Al_2O_3 catalysts Ia, IIIa, Vb, and IVb, as shown in Fig. 1.

tion of the plot $\log W_{0.5}$ versus $1/T$ using the $W_{0.5}$ values determined at different reaction temperatures (Fig. 5). The Arrhenius plots were constructed using the activity data for the 50% methane conversions that provided the same composition of the contact reaction mixture in each experiment.

The samples used for the determination of activation energy were resynthesized using the same preparation procedure. The new samples were designated as Ia*, IIa*, Va*, and Ib* where marks of I, II, and V mean the same ratios of the Pt precursor to nitric acid as those introduced in Table 1, as well as marks of a and b mean the

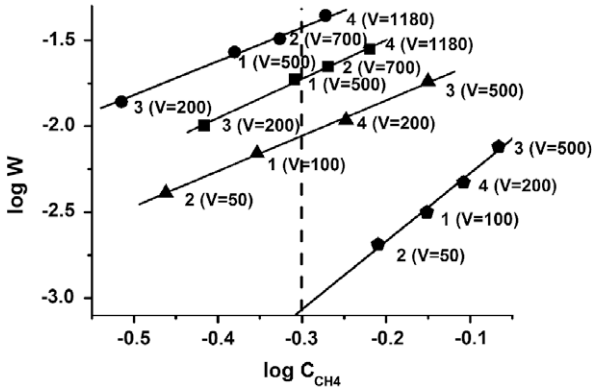

Fig. 3. The linearized log W–log C dependence for the determination of the catalytic activity of CH_4 oxidation at 700 K measured for four Pt/γ-Al_2O_3 catalysts: Ia, IIIa, Va, and Vb. The horizontal dash lines show the logarithmic values of the catalytic activity at the 50% methane conversion (log $W_{0.5}$).

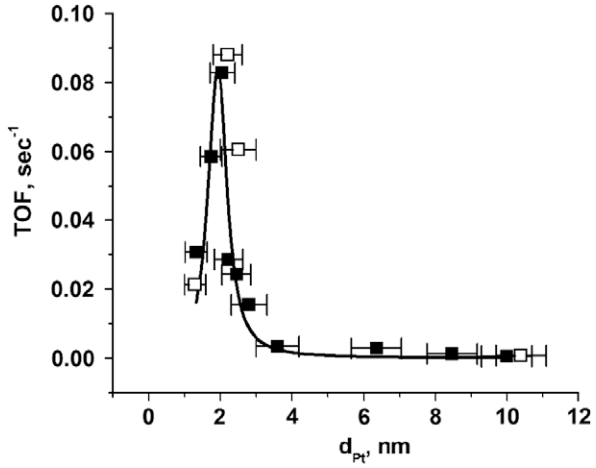

Fig. 4. Turnover frequencies in the CH_4 oxidation at 700 K as a function of the mean size of the Pt particles supported on γ-Al_2O_3. The methane conversion for all points equals 50% (see the text). The black squares are attributed to the samples listed in Table 1, while the open squares reflect the characteristics of the samples resynthesized for the activation energy measurements (see the text). Connecting curve serves merely to guide the eye.

calcination temperature of 400 and 600 °C, respectively. The mean sizes of the platinum particles in the repeatedly synthesized catalysts are shown in the Table 2. One can see that the new samples have exhibited the similar sizes of the Pt particles as the corresponding ones from the first series. This points out on good reproducibility of the preparation procedure. In full agreement with the data of Fig. 4, these samples demonstrate also similar catalytic performance (the data for new samples are shown as open squares in the same figure).

Fig. 5 shows a good linearity of the respective Arrhenius plots in the temperature range of 380 to 500 °C. The Arrhenius parameters calculated from these data show the trend of decreasing the apparent activation energy with diminishing mean particle size: 138 kJ/mol for d = 10.4 nm, 118 kJ/mol for d = 2.7 nm, 83 kJ/mol for d = 2.2 nm, and 67 kJ/mol for d = 1.3 nm. The monotonous reduction of the apparent activation energy with decreasing metal particle size has been predicted for the case of low coverage of active component with the reaction intermediates on the basis of thermodynamic analysis of the size effects in adsorption and catalysis on supported metal particles [24]. Also, as shown in [24], in that case the TOF value should increase for the catalysts with the smaller metal particles.

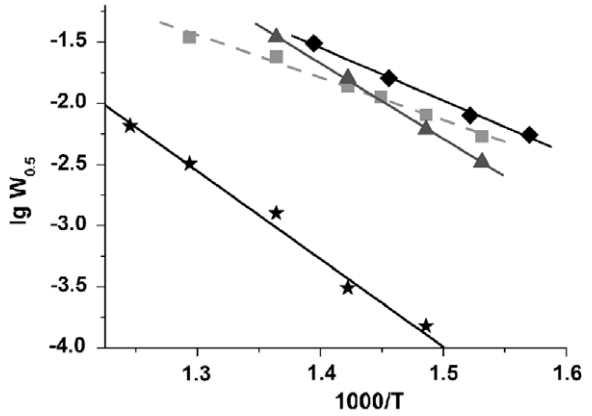

Fig. 5. Arrhenius plots for the methane oxidation for four Pt/γ-Al_2O_3 catalysts which differ in the active component size: Ia*, IIa*, Va*, and Ib*. Each value of $W_{0.5}$, the atomic catalytic activity, was determined from isothermal experiments such as those illustrated in Fig. 3.

Table 2
Some characteristics of the Pt/γ-Al_2O_3 catalysts resynthesized for the energy activation measurements.

Catalyst #	Precursor (Pt:HNO_3 ratio)	Calcination temperature (°C)	Metal loading (%)	d_{Pt} (nm)
Ia*	1:1.5	400	0.82	1.3 ± 0.4
IIa*	1:3.5	400	0.78	2.2 ± 0.4
Va*	1:0.5	400	0.74	2.5 ± 0.6
Ib*	1:1.5	600	0.67	10.4 ± 2.6

The idea on a possible thermodynamic influence on the size dependence of the catalytic reaction rate is based on a simple consideration that the standard chemical potential of small particles of condensed phase raises when their size is diminishing. Indeed, in the case of spherical particles with diameter d, their standard chemical potential $\mu(d)$ can be expressed as:

$$\mu^0(d) = \mu^0(\infty) + \frac{4\gamma V_m N_A}{d} \quad (2)$$

where $\mu^0(\infty)$ is the value of the potential for the bulk matter, γ is the excess surface energy (surface tension) on the boundary "the phase – surrounding medium", while V_m is the molecular volume of the phase. The positive increment to the standard value of chemical potential starts to be important when the increment equals or exceeds the $RT = N_A k_B T$ value, where R and k_B are the universal gas and Boltzmann constants, respectively. For typical metals, this is the case for $d \leqslant 5$ nm.

So, in case the catalytic active center is a part of the catalytically active phase matter, its chemical potential rises in the mentioned manner too. Vise versa, in case the intermediate of a catalytic transformation can be considered as a surface molecular structure which is not belonging to the phase, its chemical potential should not be dependent on the active particle size.

Such different size dependences of the chemical potentials of the active centra and of the reaction intermediates may change the potential energy barriers E_i for certain elementary catalytic transformations i, the increment in the barrier height being approximated via the Polanyi–Brönsted energy correlation like

$$E_i(r) \approx E_i + \chi \cdot \frac{4\gamma V_m N_A}{d} \quad (3)$$

where χ is a dimensionless Polanyi–Brönsted energy correlation parameter ($0 < \chi < 1$) [24].

It is of interest that for the system under study the mentioned thermodynamic approach describes nearly quantitatively the ob-

served size-dependent changes in both the TOF value at the given constant temperature and the value of apparent activation energy, E_a. Indeed, a simplified thermodynamic consideration of TOF for the low coverage of the active component with a catalytic intermediate predicts, in the ideal case of spherical particles of the active component, the following size dependence of the TOF value:

$$\mathrm{TOF}(d) = \mathrm{TOF}(\infty) \times \exp\left\{\frac{4(2-\chi)\gamma V_m}{dk_BT}\right\}. \quad (4)$$

Here, the symbols d and ∞ denote, respectively, the situations when the active component particles have size (diameter) d or are large enough ($d = \infty$), while γ is the surface tension of the active component (for Pt $\gamma \sim 2.3$ J/m^2 [27]), and V_m is the atomic volume for the active component (see above). Also, it is suggested that the rate-limiting step of the catalytic process is preceded by a quasi-equilibrated step of dissociative adsorption.

If so, one should expect a size-derived increment $\Delta E_a(d) = -\frac{4(2-\chi)\gamma V_m}{d}$ in the apparent activation energy of the overall process [24]. The same increment has to describe the change of the TOF value at the given catalyst temperature.

Fig. 6 demonstrates the experimentally observed correlation of the log (TOF) and E_a values with the reciprocal of the Pt particle sizes. It is seen that, indeed, for $d \geqslant 2$ nm a satisfactory linear correlation of both log (TOF) and E_a with $1/d$ is observed. From the experimental data on E_a it is easy to calculate (when d is expressed in nm)

$$E_a(d) = E_a(\infty) + \Delta E_a(d) \approx E_a(\infty) - \frac{105}{d}\ \mathrm{kJ/mol}, \quad (5)$$

while for the same samples at T = 700 K from the same figure it follows

$$\log\{\mathrm{TOF}(d)\} \approx \log\{\mathrm{TOF}(\infty)\} + \frac{5.17}{d}. \quad (6)$$

Note, that the experimentally derived absolute values of $\Delta E_a(d)$ in Eq. (5) are well described by the independent knowledge of parameters γ and V_m with the energy correlation coefficient $\chi = 0.75$.

Simultaneously, via comparison of (4) and (6) we obtain $\frac{4(2-\chi)\gamma V_m}{\ln 10 \cdot k_BT} = 5.17$ nm. Thus, the value of the same correlation coefficient χ, which results from independent experiment, is 1.17. Indeed, when taking into account the existence of sufficient experimental errors at the experimental determination of parameters TOF and E_a as well as extreme simplification of the model employed in [24], the obtained nearly quantitative coincidence of parameter χ derived from two independent sets of experiments (at the constant temperature and at the variation of temperature) seems to be unexpectedly excellent. Indeed, this is an important evidence in the validity of the thermodynamic approach to describe the observed size effect for Pt/γ-Al_2O_3 catalysts at least for the Pt particle size $d \geqslant 2$ nm.

It should be, however, noted that this thermodynamic approach describes only raising of the TOF with decrease in particle size from 10 to 2 nm, but not its further reduction for the catalysts with d (Pt) < 2 nm. Therefore, we did not use three data points for the approximation of the log (TOF) versus $1/d$ and for the estimation of parameter χ. At the same time, the lowest value of E_a for the Ia* catalyst (d = 1.3 nm) disagrees with its lower activity compared with that of the IIa* (d = 2.2 nm) and Va* (d = 2.5 nm) catalysts. The most probable explanation of this disagreement is the change of the reaction mechanisms and the influence of other factors on activity. As a consequence, the changes in the chemical states of active components should be proposed. To check this proposal the oxidation state of supported platinum nanoparticles and the local structure of the active component in the samples used for the determination of Ea have been studied by XAFS.

3.4. Change of the supported Pt local structure with the particle size

Figs. 7 and 8 show the normalized XANES spectra (Pt–L_3 edge, * – white line) and RDFs describing the Pt local arrangements, respectively, for three catalysts differing in the Pt particle sizes (samples Ia*, IIa*, and Ib*) as well as for two reference samples (Pt foil and PtO_2).

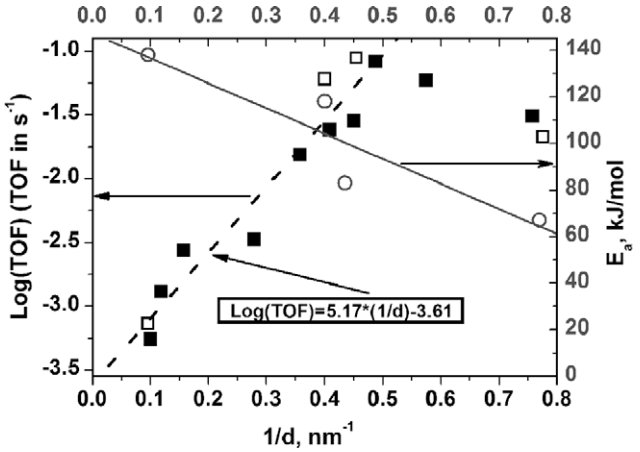

Fig. 6. The correlation of the measured TOF values at a temperature of 700 K and of the apparent activation energies E_a with the reciprocal to the active component size (diameter) d.

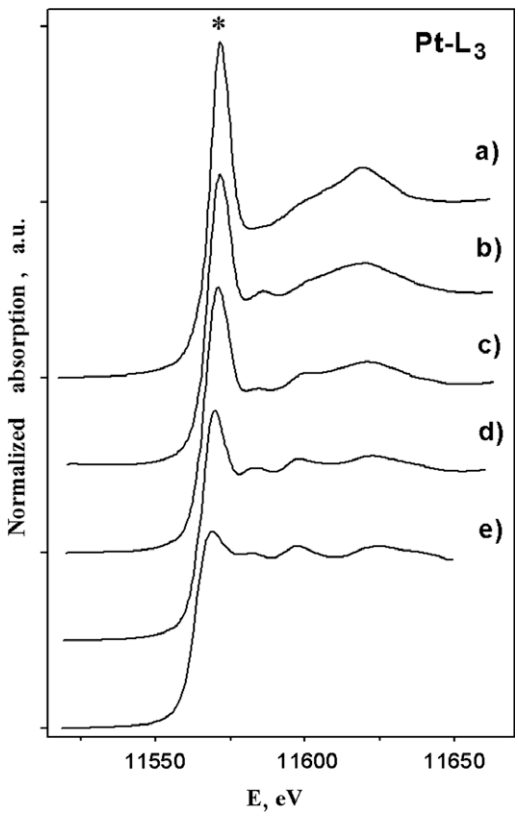

Fig. 7. XANES spectra (Pt–L_3 edge) of the references and three Pt/γ-Al_2O_3 catalysts which differ in the active component size: (a) bulk PtO_2; (b) sample Ia* (d ca. 1.3 nm); (c) sample IIa* (d ca. 2.2 nm); (d) sample Ib* (d ca. 10.4 nm); and (e) Pt foil.

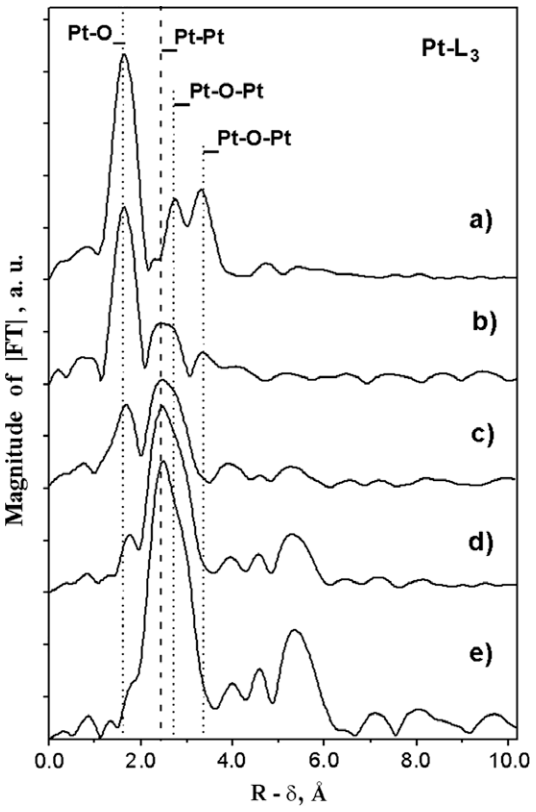

Fig. 8. Radial distribution functions (RDFs) of atoms describing the Pt local arrangement for the references and three Pt/γ-Al_2O_3 catalysts which differ in the active component size: (a) bulk PtO_2; (b) sample Ia* (*d* ca. 1.3 nm); (c) sample IIa* (*d* ca. 2.2 nm); (d) sample Ib* (*d* ca. 10.4 nm); and (e) Pt foil.

The white line intensity and the shape and features of the XANES (Pt–L_3) spectra clearly indicate some differences in the oxidation state of the supported Pt particles [28] in the catalyst samples under the study (Fig. 7b–d). A pronounced tendency of transformation of the XANES spectra from the PtO_2 reference (Fig. 7a) to the Pt foil (Fig. 7e) is observed for the samples studied (Fig. 7b–d) when the mean particle size increases from 1.3 (Ia*) to 2.2 nm (IIa*) and further to 10.4 nm (Ib*). In addition to the decrease of the white line amplitudes in the series, a shift of the edge position of the spectra to lower values of photon energy was observed. Since amplitude of the white line is associated directly with the amount of oxidized platinum [28], these data indicate that the increase in the Pt particle size reduces the fraction of the oxidized form of platinum in the samples. Indeed, the XANES spectra of the sample with the largest Pt particles (Fig. 7d) are rather similar to the spectrum of a Pt foil reference (Fig. 7e), whereas the spectra of the other samples (Fig. 7b and c) exhibit features from both the PtO_2 (Fig. 7a) and Pt^0 (Fig. 7e) references.

Comparison of the radial distribution functions calculated for the same catalysts and RDFs of the reference samples confirm the above conclusion (Fig. 8). A pronounced set of metallic Pt–Pt peaks is observed on the RDF curve of the reference Pt foil (Fig. 8e). The main peak corresponds to the shortest Pt–Pt distance of 2.77 Å with the coordination number (CN) of 12 that is typical for a fcc structure [29]. The first intensive peak on the RDF curve of the PtO_2 reference (Fig. 8a) corresponds to the Pt–O distance ($R_{Pt-O} \sim 2.0$ Å, CN ~ 6.0) [30]. The next two less intensive peaks on the RDF curve of PtO_2 may be attributed to several Pt–(O)–Pt distances in platinum oxide ($R_{Pt-Pt} \sim 3.0$ to 4.0 Å).

It should be noted that the similar peaks corresponding to the shortest first Pt–O (R = 2.0 Å) and shortest first Pt–Pt (R = 2.75 Å) distances, which are typical for the oxide and metal phases, were observed on the RDF curves of the supported Ia* (Fig. 8b) and IIa* (Fig. 8c) Pt/Al_2O_3 catalysts. The first peak position (R = 1.99 Å) for both samples is similar to that of the PtO_2 reference (Fig. 8a) and should be assigned to the direct Pt–O distances. At the same time the intensity of this peak differs more drastically and results in the estimation of CN as ca. 4.4 for the Ia* and ca. 2.1 for the IIa* sample. Fitting for the second peak corresponding to the Pt–Pt distances in metal phase leads to R = 2.73 Å, CN = 2.6 and R = 2.74 Å, CN = 5.6 for the Ia* and IIa* samples (Fig. 8b and c), respectively.

On the other hand, the RDF curve for the Ib* sample with the largest Pt particles (Fig. 8d) exhibits predominantly the metallic character of the active phase giving rise to one main peak on the RDF curve corresponding to the first Pt–Pt (R = 2.75 Å, CN ~ 9) distance as well as to a pronounced set of other metallic Pt–Pt peaks which are similar to peaks of the Pt foil. No oxidized platinum is detected in this sample Ib* (Fig. 8d) within the XAFS method limitation.

Therefore, a gradual change both in the features of supported platinum from ionic to metallic one and in specific catalytic activity in methane oxidation occurs with an increase in the particle size. The above data allow us to suggest two possible explanations for the unusual size sensitivity depending on the real nature of the catalytically active species: metallic platinum or partially oxidized one.

If only metallic species are active [14], the bell-shaped size dependence (Fig. 4) can be assigned to the competition between the increase in the chemical potential of the active centra with the decrease in the particle size, which lowers the barrier of CH_4 activation, on the one hand, and the increase in the part of catalytically active Pt^0 particles with the particle enlargement, on the other hand.

If the second hypothesis is correct, the combination of comparable amounts of the oxidized and metallic platinum species for the catalysts with *d* (Pt) of ca. 2 nm (Figs. 7 and 8) can set conditions for the maximum activity in the methane oxidation, in full accordance with [25,26]. In this case, the observed decrease in the TOF value (Fig. 4) with the change in the active phase size seems to be caused by the change in the Pt^0/PtO_x ratio toward the predominance of either oxidized Pt species (at d < 2 nm) or metallic species (at d > 2 nm).

4. Conclusions

Oligomeric μ-hydroxo Pt(IV) complexes obtained in aqueous solutions which differ in Pt:HNO_3 ratio can be used for the size-controlled and well reproducible formation of supported platinum nanoparticles if they are applied for the impregnation of acid-pretreated γ-alumina. The additional parameter which regulates the mean sizes of platinum particles is the calcination temperature. Using these parameters, a set of the Pt/γ-Al_2O_3 catalysts with the mean particle sizes ranged from 1 to 10 nm and narrow size distribution has been synthesized. The methane total oxidation on these chlorine-free Pt/γ-Al_2O_3 catalysts is shown to be strongly size sensitive. The size dependence of the TOF is narrow and bell-shaped. The maximal TOF value is observed for the Pt crystallites of ca. 2 nm containing comparable amounts of partially oxidized and metallic platinum species.

For the catalysts with the Pt nanoparticle size above 2 nm when platinum is predominantly in metallic state, the observed size dependence of the TOF value originates from the size dependence of the apparent activation energy of the process and is well described by a simple thermodynamic approach [24] for metallic particles. The observed decrease in the TOF value at diminishing Pt nanoparticle sizes below 2 nm seems to be due to predomi-

nantly non-metallic nature of so fine platinum particles because of a strong interaction with the support.

Acknowledgments

This work was partially supported by Russian Science and Innovation Agency (contracts #02.513.11.3203 and 02.518.11.7128), RFBR (projects #08-03-01016, 08-03-01150, and 09-03-01012), and RAS Presidium (grants #27.12 and 27.51).

References

[1] R.A. Van Santen, Acc. Chem. Res. 42 (2009) 57.
[2] A.K. Santra, D.W. Goodman, Electrochim. Acta 47 (2002) 3595.
[3] T.F. Garetto, C.R. Apesteguia, Appl. Catal. B – Environ. 32 (2001) 83.
[4] P. Gelin, M. Primet, Appl. Catal. B – Environ. 39 (2002) 1.
[5] T.F. Garetto, C.R. Apesteguia, Catal. Today 62 (2000) 189.
[6] L. Burch, P.K. Loader, Appl. Catal. B – Environ. 5 (1994) 149.
[7] M. Kobayashi, T. Kanno, A. Konishi, H. Takeda, React. Kinet. Catal. Lett. 37 (1988) 89.
[8] Y.-F.Y. Yao, Ind. Eng. Chem. Prod. Res. Dev. 19 (1980) 293.
[9] P. Briot, A. Auroux, D. Jones, M. Primet, Appl. Catal. 59 (1990) 141.
[10] M. Niwa, K. Awano, Y. Murakami, Appl. Catal. 7 (1983) 317.
[11] E. Marceau, M. Che, J. Saint-Just, J.M. Tatibouët, Catal. Today 29 (1996) 415.
[12] V.A. Drozdov, P.G. Tsyrulnikov, V.V. Popovskii, N.N. Bulgakov, E.M. Moroz, T.G. Galeev, React. Kinet. Catal. Lett. 27 (1985) 425.
[13] D.O. Simone, T. Kennely, N.L. Brungard, R.J. Farrauto, Appl. Catal. 70 (1991) 87.
[14] R.F. Hicks, H. Qi, M.L. Young, R.G. Lee, J. Catal. 122 (1990) 280.
[15] R.F. Hicks, H. Qi, M.L. Young, R.G. Lee, W.J. Han, A.B. Kooh, Chem. Eng. Sci. 45 (1990) 2647.
[16] K. Otto, Langmuir 5 (1989) 1364.
[17] D.I. Kochubey, EXAFS Spectroscopy of Catalysts, Nauka, Novosibirsk, 1992.
[18] K.V. Klementiev, code VIPER for Windows, freeware: <www.desy.de/~klmn/viper.html>.
[19] N. Binsted, J.V. Campbell, S.J. Gurman, P.C. Stephenson, EXCURV92, Daresb. Lab., UK, 1991.
[20] N.N. Bobrov, V.N. Parmon, in: NATO Science Series II: Mathematics, Physics and Chemistry, vol. 69, Kluwer, 2002, p. 197.
[21] J.R. Anderson, Structure of Metallic Catalysts, Academic Press, London, 1975. p. 296.
[22] C.O. Bennett, M. Che, J. Catal. 120 (1989) 293.
[23] D. Farin, D. Avnir, J. Am. Chem. Soc. 110 (1988) 2039.
[24] V.N. Parmon, Dokl. Phys. Chem. 413 (2007) 42.
[25] R. Burch, M.J. Hayes, J. Mol. Catal. A 100 (1995) 13.
[26] E. Becker, P.-A. Carlsson, H. Grönbeck, M. Skoglundh, J. Catal. 252 (2007) 11.
[27] G. Somorjai, Introduction to Surface Chemistry and Catalysis, Wiley, NY, 1994. p. 274.
[28] H. Yoshida, S. Nonoyama, Y. Yazawa, T. Hattori, Phys. Scr. 115 (2005) 813.
[29] ICSD/Retrieve Codes: Pt^0 – 76153.
[30] ICSD/Retrieve Codes: α-PtO_2 – 24922, 24923.